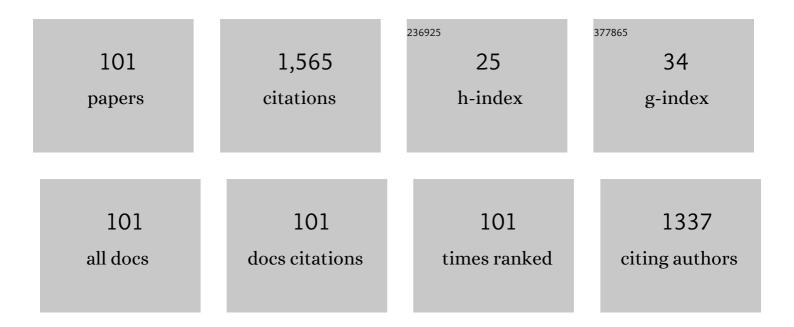
Atsushi Okamoto

List of Publications by Year in descending order

Source: https://exaly.com/author-pdf/362548/publications.pdf Version: 2024-02-01



#	Article	IF	CITATIONS
1	Volatile-consuming reactions fracture rocks and self-accelerate fluid flow in the lithosphere. Proceedings of the National Academy of Sciences of the United States of America, 2022, 119, .	7.1	8
2	Machine-learning techniques for quantifying the protolith composition and mass transfer history of metabasalt. Scientific Reports, 2022, 12, 1385.	3.3	1
3	Continental arc-derived eclogite in the Zavkhan Terrane, western Mongolia: Implications for the suture zone in the northern part of the Central Asian Orogenic Belt. Journal of Asian Earth Sciences, 2022, 229, 105150.	2.3	4
4	Redistribution of magnetite during multi–stage serpentinization: Evidence from the Taishir Massif, Khantaishir ophiolite, western Mongolia. Journal of Mineralogical and Petrological Sciences, 2021, 116, 176-181.	0.9	2
5	Formation of amorphous silica nanoparticles and its impact on permeability of fractured granite in superhot geothermal environments. Scientific Reports, 2021, 11, 5340.	3.3	7
6	Multi-stage infiltration of Na- and K-rich fluids from pegmatites at mid-crustal depths as revealed by feldspar replacement textures. Lithos, 2021, 388-389, 106096.	1.4	5
7	1-D inversion analysis of a shallow landslide triggered by the 2018 Eastern Iburi earthquake in Hokkaido, Japan. Earth, Planets and Space, 2021, 73, .	2.5	4
8	Albite–K-feldspar–quartz equilibria in hydrothermal fluids at 400, 420°C and 20–35 MPa: Experimental measurements and thermodynamic calculations. Geothermics, 2021, 94, 102109.	3.4	6
9	Rupture of wet mantle wedge by self-promoting carbonation. Communications Earth & Environment, 2021, 2, .	6.8	28
10	Crucial Scientific Issues in Earth Science Revealed Only by Mantle Drilling: Understanding the Current State of the Oceanic Plates of a Life-bearing Planet. Journal of Geography (Chigaku Zasshi), 2021, 130, 483-506.	0.3	2
11	Experimental fracture sealing in reservoir sandstones and its relation to rock texture. Journal of Structural Geology, 2021, 153, 104447.	2.3	7
12	Cataclastic and crystal-plastic deformation in shallow mantle-wedge serpentinite controlled by cyclic changes in pore fluid pressures. Earth and Planetary Science Letters, 2021, 576, 117232.	4.4	5
13	Hadal aragonite records venting of stagnant paleoseawater in the hydrated forearc mantle. Communications Earth & Environment, 2021, 2, .	6.8	6
14	Multi-stage serpentinization of ultramafic rocks in the Manlay Ophiolite, southern Mongolia. Mongolian Geoscientist, 2021, 26, 1-17.	0.3	1
15	Impact of fluid pressure on failure mode in shear zones: Numerical simulation of en-echelon tensile fracturing and transition to shear. Tectonophysics, 2020, 774, 228277.	2.2	2
16	Stabilizing and enhancing permeability for sustainable and profitable energy extraction from superhot geothermal environments. Applied Energy, 2020, 260, 114306.	10.1	33
17	Silica controls on hydration kinetics during serpentinization of olivine: Insights from hydrothermal experiments and a reactive transport model. Geochimica Et Cosmochimica Acta, 2020, 270, 21-42.	3.9	18
18	Inferring fracture forming processes by characterizing fracture network patterns with persistent homology. Computers and Geosciences, 2020, 143, 104550.	4.2	12

#	Article	IF	CITATIONS
19	Fluid Infiltration Through Oceanic Lower Crust in Response to Reactionâ€Induced Fracturing: Insights From Serpentinized Troctolite and Numerical Models. Journal of Geophysical Research: Solid Earth, 2020, 125, e2020JB020268.	3.4	15
20	Crystallographic preferred orientation of talc determined by an improved EBSD procedure for sheet silicates: Implications for anisotropy at the slab–mantle interface due to Si-metasomatism. American Mineralogist, 2020, 105, 873-893.	1.9	9
21	Transport and Evolution of Supercritical Fluids During the Formation of the Erdenet Cu–Mo Deposit, Mongolia. Geosciences (Switzerland), 2020, 10, 201.	2.2	3
22	Thermodynamic modeling of hydrous-melt–olivine equilibrium using exhaustive variable selection. Physics of the Earth and Planetary Interiors, 2020, 300, 106430.	1.9	10
23	Characteristics of hydrogen production with carbon storage by CO2-rich hydrothermal alteration of olivine in the presence of Mg–Al spinel. International Journal of Hydrogen Energy, 2020, 45, 13163-13175.	7.1	5
24	Rapid fluid infiltration and permeability enhancement during middle–lower crustal fracturing: Evidence from amphibolite–granulite-facies fluid–rock reaction zones, SÃ,r Rondane Mountains, East Antarctica. Lithos, 2020, 372-373, 105521.	1.4	14
25	Chemical Reactions in Subsurface Storage Rocks - First Results from Reactive Fluid Flow Experiments. , 2020, , .		0
26	Silica nanoparticles produced by explosive flash vaporization during earthquakes. Scientific Reports, 2019, 9, 9738.	3.3	12
27	Geological and engineering features of developing ultra-high-temperature geothermal systems in the world. Geothermics, 2019, 82, 267-281.	3.4	27
28	Formation of secondary olivine after orthopyroxene during hydration of mantle wedge: evidence from the Khantaishir Ophiolite, western Mongolia. Contributions To Mineralogy and Petrology, 2019, 174, 1.	3.1	12
29	Pyroxene control of H2 production and carbon storage during water-peridotite-CO2 hydrothermal reactions. International Journal of Hydrogen Energy, 2019, 44, 26835-26847.	7.1	9
30	NaHCO3-promoted olivine weathering with H2 generation and CO2 sequestration in alkaline hydrothermal system. IOP Conference Series: Earth and Environmental Science, 2019, 257, 012017.	0.3	1
31	Melt–fluid infiltration along detachment shear zones in oceanic core complexes: Insights from amphiboles in gabbro mylonites from the Godzilla Megamullion, Parece Vela Basin, the Philippine Sea. Lithos, 2019, 344-345, 217-231.	1.4	18
32	Acceleration of hydrogen production during water-olivine-CO2 reactions via high-temperature-facilitated Fe(II) release. International Journal of Hydrogen Energy, 2019, 44, 11514-11524.	7.1	9
33	Enhanced hydrogen production with carbon storage by olivine alteration in CO2-rich hydrothermal environments. Journal of CO2 Utilization, 2019, 30, 205-213.	6.8	11
34	Al-Zoning of Serpentine Aggregates in Mesh Texture Induced by Metasomatic Replacement Reactions. Journal of Petrology, 2018, 59, 613-634.	2.8	12
35	Multiple Kinetic Parameterization in a Reactive Transport Model Using the Exchange Monte Carlo Method. Minerals (Basel, Switzerland), 2018, 8, 579.	2.0	5
36	Recovering the past history of natural recording media by Bayesian inversion. Physical Review E, 2018, 98, .	2.1	7

#	Article	IF	CITATIONS
37	Loop energy: A useful indicator of the hardness of minerals from depth-sensing indentation tests. Journal of Structural Geology, 2018, 117, 96-104.	2.3	4
38	Potentially exploitable supercritical geothermal resources in the ductile crust. Nature Geoscience, 2017, 10, 140-144.	12.9	96
39	Excess water generation during reaction-inducing intrusion of granitic melts into ultramafic rocks at crustal P–T conditions in the Sør Rondane Mountains of East Antarctica. Lithos, 2017, 284-285, 625-641.	1.4	12
40	Porosity and Permeability Evolution Induced by Precipitation of Silica under Hydrothermal Conditions. Procedia Earth and Planetary Science, 2017, 17, 249-252.	0.6	5
41	In Situ Observation of Critical Phenomena of Multicomponent Geofluids and Seawater by Using Visible-type Autoclave. Procedia Earth and Planetary Science, 2017, 17, 296-299.	0.6	0
42	Mechanisms of Serpentinization Utilizing Olivine–Plagioclase–H2O System under Hydrothermal Conditions. Procedia Earth and Planetary Science, 2017, 17, 686-689.	0.6	3
43	Silica precipitation potentially controls earthquake recurrence in seismogenic zones. Scientific Reports, 2017, 7, 13337.	3.3	21
44	Fluid Pocket Generation in Response to Heterogeneous Reactivity of a Rock Fracture Under Hydrothermal Conditions. Geophysical Research Letters, 2017, 44, 10,306.	4.0	13
45	Reaction-induced grain boundary cracking and anisotropic fluid flow during prograde devolatilization reactions within subduction zones. Contributions To Mineralogy and Petrology, 2017, 172, 1.	3.1	8
46	Opal T in chert beneath the toe of the Tohoku margin and its influence on the seismic aseismic transition in subduction zones. Geophysical Research Letters, 2017, 44, 687-693.	4.0	2
47	Information extraction from metamorphic rock textures and compositional zoning of minerals:. Journal of the Geological Society of Japan, 2017, 123, 733-745.	0.6	2
48	Contrast in stress–strain history during exhumation between high- and ultrahigh-pressure metamorphic units in the Western Alps: Microboudinage analysis of piemontite in metacherts. Journal of Structural Geology, 2016, 89, 168-180.	2.3	5
49	Bayesian inversion analysis of nonlinear dynamics in surface heterogeneous reactions. Physical Review E, 2016, 94, 033305.	2.1	10
50	The roles of fluid transport and surface reaction in reaction-induced fracturing, with implications for the development of mesh textures in serpentinites. Contributions To Mineralogy and Petrology, 2016, 171, 1.	3.1	23
51	Reaction-induced rheological weakening enables oceanic plate subduction. Nature Communications, 2016, 7, 12550.	12.8	39
52	Phaseâ€field modeling of epitaxial growth of polycrystalline quartz veins in hydrothermal experiments. Geofluids, 2016, 16, 211-230.	0.7	38
53	Contrasting geochemical signatures of Devonian and Permian granitoids from the Tseel Terrane, SW Mongolia. Journal of Geosciences (Czech Republic), 2016, , 51-66.	0.6	9
54	Free-energy landscape and nucleation pathway of polymorphic minerals from solution in a Potts lattice-gas model. Physical Review E, 2015, 92, 042130.	2.1	6

#	Article	IF	CITATIONS
55	Beyondâ€laboratoryâ€scale prediction for channeling flows through subsurface rock fractures with heterogeneous aperture distributions revealed by laboratory evaluation. Journal of Geophysical Research: Solid Earth, 2015, 120, 106-124.	3.4	64
56	Contrasting fracture patterns induced by volume-increasing and -decreasing reactions: Implications for the progress of metamorphic reactions. Earth and Planetary Science Letters, 2015, 417, 9-18.	4.4	27
57	Competitive hydration and dehydration at olivine–quartz boundary revealed by hydrothermal experiments: Implications for silica metasomatism at the crust–mantle boundary. Earth and Planetary Science Letters, 2015, 425, 44-54.	4.4	17
58	Possibility to remedy CO2 leakage from geological reservoir using CO2 reactive grout. International Journal of Greenhouse Gas Control, 2014, 20, 310-323.	4.6	30
59	Thermal evolution of the <scp>T</scp> seel terrane, <scp>SW</scp> Mongolia and its relation to granitoid intrusions in the <scp>C</scp> entral <scp>A</scp> sian <scp>O</scp> rogenic <scp>B</scp> elt. Journal of Metamorphic Geology, 2014, 32, 765-790.	3.4	35
60	Rheological properties of the detachment shear zone of an oceanic core complex inferred by plagioclase flow law: Godzilla Megamullion, Parece Vela back-arc basin, Philippine Sea. Earth and Planetary Science Letters, 2014, 408, 16-23.	4.4	13
61	The significance of silica precipitation on the formation of the permeable–impermeable boundary within Earth's crust. Terra Nova, 2014, 26, 253-259.	2.1	49
62	Distribution of CO2 fluids in the Shimanto belt on Muroto Peninsula, SW Japan: possible injection of magmatic CO2 into the accretionary prism. Earth, Planets and Space, 2014, 66, .	2.5	6
63	Radiocarbon Dating Historical Tsunami Deposits from the Sendai Plain, Northeastern Japan: Preliminary Age Model of HS Continuous Soil Sediment Series. Journal of Geography (Chigaku Zasshi), 2014, 123, 904-922.	0.3	13
64	Seawater-leaching Testing for Arsenic and Heavy Metals in Tsunami Deposits Produced by the 2011 off the Pacific Coast of Tohoku Earthquake, Northeastern Japan. Journal of Geography (Chigaku Zasshi), 2014, 123, 835-853.	0.3	10
65	Millimeter– to decimeter–scale compositional mapping using a scanning X–ray analytical microscope and its application to a reaction zone in high–grade metamorphic rock. Journal of Mineralogical and Petrological Sciences, 2014, 109, 271-278.	0.9	5
66	Vein texture: a window for fluid dynamics in the crust. Ganseki Kobutsu Kagaku, 2014, 43, 25-29.	0.1	2
67	The Effect of Al and Na on the Precipitation Rate of Silica Minerals: Hydrothermal Flow-Through Experiments at 430°C and 31MPa. Procedia Earth and Planetary Science, 2013, 7, 762-765.	0.6	3
68	Effect of Silica Transport on Serpentinization in the Ol-Opx- H2O System. Procedia Earth and Planetary Science, 2013, 7, 628-631.	0.6	3
69	Coupled reactions and silica diffusion during serpentinization. Geochimica Et Cosmochimica Acta, 2013, 119, 212-230.	3.9	44
70	Spectroscopic determination of the critical temperatures and pressures of H2O, CO2, and C2H5OH. Journal of Mineralogical and Petrological Sciences, 2013, 108, 356-361.	0.9	2
71	Distribution of artificial radionuclides (110mAg, 129mTe, 134Cs, 137Cs) in surface soils from Miyagi Prefecture, northeast Japan, following the 2011 Fukushima Dai-ichi nuclear power plant accident. Geochemical Journal, 2012, 46, 279-285.	1.0	30
72	Mineralogical variation of silica induced by Al and Na in hydrothermal solutions. American Mineralogist, 2012, 97, 2060-2063.	1.9	9

#	Article	IF	CITATIONS
73	An exhumation pressure–temperature path and fluid activities during metamorphism in the Tseel terrane, SW Mongolia: Constraints from aluminosilicate-bearing quartz veins and garnet zonings in metapelites. Journal of Asian Earth Sciences, 2012, 54-55, 214-229.	2.3	12
74	GeoFlow: A novel model simulator for prediction of the 3â€Ð channeling flow in a rock fracture network. Water Resources Research, 2012, 48, .	4.2	28
75	Risk assessments of Arsenic in tsunami sediments from Iwate, Miyagi and Fukushima Prefectures, Northeast Japan, by the 2011 off the Pacific coast of Tohoku Earthquake. Journal of the Geological Society of Japan, 2012, 118, 419-430.	0.6	29
76	Progress of hydration reactions in olivine–H2O and orthopyroxenite–H2O systems at 250 °C and vapor-saturated pressure. Chemical Geology, 2011, 289, 245-255.	3.3	58
77	Thermodynamic forward modeling of progressive dehydration reactions during subduction of oceanic crust under greenschist facies conditions. Earth and Planetary Science Letters, 2011, 307, 9-18.	4.4	20
78	Application of the microboudin method to palaeodifferential stress analysis of deformed impure marbles from Syros, Greece: Implications for grain-size and calcite-twin palaeopiezometers. Journal of Structural Geology, 2011, 33, 20-31.	2.3	7
79	Textures of syntaxial quartz veins synthesized by hydrothermal experiments. Journal of Structural Geology, 2011, 33, 1764-1775.	2.3	41
80	In situ observation of the crystallization pressure induced by halite crystal growth in a microfluidic channel. American Mineralogist, 2011, 96, 1012-1019.	1.9	18
81	Determination of amphibole fracture strength for quantitative palaeostress analysis using microboudinage structures. Journal of Structural Geology, 2010, 32, 136-150.	2.3	6
82	Mineralogical and textural variation of silica minerals in hydrothermal flow-through experiments: Implications for quartz vein formation. Geochimica Et Cosmochimica Acta, 2010, 74, 3692-3706.	3.9	53
83	Velocity of vertical fluid ascent within vein-forming fractures. Geology, 2009, 37, 563-566.	4.4	33
84	Development of Discrete Fracture Network Model Simulator, GeoFlow, for Evaluation of Three Dimensional Channeling Flow. , 2009, , .		2
85	Mineral distribution within polymineralic veins in the Sanbagawa belt, Japan: implications for mass transfer during vein formation. Contributions To Mineralogy and Petrology, 2008, 156, 323-336.	3.1	28
86	Magnitude of σ1, σ2, and σ3 at mid-crustal levels in an orogenic belt: Microboudin method applied to an impure metachert from Turkey. Tectonophysics, 2008, 460, 230-236.	2.2	10
87	Effect Of Lithology On Calcite-Vein Formation In The Sanbagawa Metamorphic Rocks. AIP Conference Proceedings, 2008, , .	0.4	Ο
88	Variations in stable isotope compositions (δ13C, δ18O) of calcite within exhumation-related veins from the Sanbagawa metamorphic belt. Journal of Mineralogical and Petrological Sciences, 2008, 103, 361-364.	0.9	7
89	Mineral Growth within Fluid-filled Cracks: Example of Polymineralic Veins from the Sanbagawa Metamorphic Belt, Japan. AIP Conference Proceedings, 2007, , .	0.4	0
90	Variable microstructure of peridotite samples from the southern Mariana Trench: Evidence of a complex tectonic evolution. Tectonophysics, 2007, 444, 111-118.	2.2	43

#	Article	IF	CITATIONS
91	Cessation of plastic deformation during exhumation of metamorphic tectonites revealed by microboudinage structures. Journal of Structural Geology, 2007, 29, 159-165.	2.3	8
92	Seismic anisotropy in the uppermost mantle, back-arc region of the northeast Japan arc: Petrophysical analyses of Ichinomegata peridotite xenoliths. Geophysical Research Letters, 2006, 33, n/a-n/a.	4.0	26
93	Misorientations of garnet aggregate within a vein: an example from the Sanbagawa metamorphic belt, Japan. Journal of Metamorphic Geology, 2006, 24, 353-366.	3.4	7
94	Reaction progress related to indentation structures at glaucophane/glaucophane contacts in an impure marble from Syros, Greece. Journal of Metamorphic Geology, 2006, 24, 703-713.	3.4	1
95	Rapid Growth of Garnet within a Metamorphic Vein Inferred from Misorientation Angle Distribution of Garnet Porphyroblasts. AIP Conference Proceedings, 2006, , .	0.4	Ο
96	Progress of actinolite-forming reactions in mafic schists during retrograde metamorphism: an example from the Sanbagawa metamorphic belt in central Shikoku, Japan. Journal of Metamorphic Geology, 2005, 23, 335-356.	3.4	40
97	Progressive shape evolution of a mineral inclusion under differential stress at high temperature: Example of garnet inclusions within a granulite-facies quartzite from the Lützow-Holm Complex, East Antarctica. Journal of Geophysical Research, 2005, 110, .	3.3	13
98	Triaxial stress state deep in orogenic belts: an example from Turkey. Journal of Structural Geology, 2004, 26, 2203-2209.	2.3	7
99	Optimal mixing properties of calcic and subcalcic amphiboles: application of Gibbs? method to the Sanbagawa schists, SW Japan. Contributions To Mineralogy and Petrology, 2004, 146, 529-545.	3.1	48
100	Orientation contrast images of garnet in granulite-facies quartzite, Lützow-Holm Complex, East Antarctica. Journal of the Geological Society of Japan, 2004, 110, V-VI.	0.6	6
101	Application of differential thermodynamics (Gibbs' method) to amphibole zonings in the metabasic system. Contributions To Mineralogy and Petrology, 2001, 141, 268-286.	3.1	26